MHz Ultrasound Induced Roughness of Fluid Interfaces

Rym Boubekri, Michel Gross, Martin In, Olivier Diat, Maurizio Nobili, Helmuth Moehwald, Antonio Stocco

MHz ultrasound induced roughness of fluid interfaces

Rym Boubekri,[1,2] Michel Gross,[1] Martin In,[1] Olivier Diat,[2] Maurizio Nobili,[1] Helmuth Möhwald,[3,*] Antonio Stocco[1,**]

[1]Laboratoire Charles Coulomb (L2C), UMR 5221 CNRS-Univ. Montpellier , Montpellier F-34095, France.**Antonio.Stocco@umontpellier.fr

[2]Institut de Chimie Séparative de Marcoule, UMR 5257 (CEA, CNRS, UM, ENSCM), BP 17171, 30207 Bagnols-sur-Cèze Cedex, France.

[3]Max-Planck-Institute of Colloids and Interfaces, Am Mühlenberg, 14476 Potsdam, Germany. *Helmuth.Moehwald@mpikg.mpg.de

ABSTRACT

The interface between two fluids is never flat at the nanoscale, and this is important for transport across interfaces. In absence of any external field, the surface roughness is due to thermally excited capillary waves possessing subnanometric amplitudes in the case of simple liquids. Here, we investigate the effect of ultrasound on the surface roughness of liquid-gas and liquid-liquid interfaces. MHz frequency ultrasound was applied normal to the interface at relatively low ultrasonic pressures (< 0.6 MPa), and the amplitudes of surface fluctuations have been measured by light reflectivity and ellipsometry. We found a dramatic enhancement of surface roughness, roughly linear with intensity, with vertical displacements of the interface as high as 50-100 nm. As a consequence, the effective contact area between two fluids can be increased by ultrasound. This result has a clear impact for enhancing interface based processes such as mass or heat transfer.

1. INTRODUCTION

Ultrasound (US) is widely used in chemistry as it is applicable to any medium without direct contact. The most frequent application with frequencies between 20 kHz and some MHz is cleaning and effecting chemical reactions, making use of the extreme conditions of temperature and pressure upon cavitation and liquid movement following bubble collapse, so called ultrasonic streaming. Frequencies above some MHz are used for imaging diagnostics, whereas a broad range of frequencies is used for spectroscopy, based on the kinetics of local movement or changes, e.g. of a hydration shell. Many applications have in common, that US is reflected or absorbed at interfaces between two phases due to a difference in density and/or elastic modulus. Therefore at high pressures the interfaces may be destabilized, and this is used in emulsification. For less strong US absorption this destabilization may be less pronounced, and in this case one may still expect, that an interfacial reaction can be enhanced without macroscopically or permanently destabilizing the interface. A typical system, where this is desirable are microfluidic devices where phase transfer should be accelerated while still recovering the individual phases after this transfer.[1] This case is studied in this work, where a fluid interface is exposed to an US wave perpendicular to it, which tends to modify its fluctuation pattern. Gravity and interfacial tension act as restoring forces. The case studied here

is relevant for acoustic emulsification[2] and ultrasonic atomization,[3] where the interface deformation is a first step of droplet formation. In the following steps of acoustic emulsification, the surface instability grows rapidly and leads to the formation of droplets, whose sizes are very similar to the wavelength of the surface waves excited by US.[2,4] In ultrasonic atomization, the drop size strongly depends on the frequency: $D = 0.34\ [8\pi\gamma/(\rho f^2)]^{1/3}$ (where γ is the interfacial tension, ρ is the density and f the US frequency).[5] Nebulizers or emulsification apparatus operating at MHz frequencies lead to the formation of droplets in the micron range in agreement with capillary wave theory.[6,7] One additional remarkable observation in acoustic emulsification is the very high stability of the droplets in absence of any surface active species. US may in fact induce charging of a fluid interface, and an enrichment of hydroxide ions at the interface, which stabilize electrostatically the droplets against coalescence.[8]

The potential of US to enhance a phase transfer reaction and liquid-liquid extraction has motivated the present study, which focuses on the US induced surface roughness with frequency in the MHz range and in a range of intensities, where surface deformation remains small and acoustic cavitation does not occur.[9] Hence, we focus our attention on the first step of ultrasonic atomization and acoustic emulsification and aim at evaluating the amplitude of surface roughness and the interfacial profile as a function of the US pressure.

The experimental setup, methods and systems under investigation are described in section 2. Light reflectivity and ellipsometry (section 3) were used to evaluate the interfacial profile of the fluid interfaces. Surface roughness induced by US and measured by light reflectivity shows an enhancement of the amplitude by two orders of magnitude when compared to thermally excited capillary waves.

2. EXPERIMENTAL METHODS

2.1. SETUP

A transducer (Olympus, Panametrics, A305S), diameter D = 19 mm, frequency f = 2.25 MHz, wavelength λ_{US} =0.66 mm, was used to generate ultrasound in water and towards the liquid interface and being placed at the focal distance l_f to it (focal length = l_f = 75 mm). The transducer was connected to a waveform generator (Rigol DG1000) and an analogue Oscilloscope (Hameg Instruments, HM303-6), see Fig. 1.

The acoustic wave is emitted for times of several seconds (about 1 minute), which corresponds to the acquisition time for our optical experiments. We investigated for pressure maxima P up to 0.58 MPa (about 5.7 atm). Pressure calibration was done using two different hydrophones (Precision Acoustics, UK) of 0.5 mm and 0.2 mm diameter submerged in water at a distance equal to the focal length of the US transducer.

To calculate the profile of the pressure field at the focal plane $P_0(r)$ generated by the US transducer in water we used the expression for a spherical transducer.[10]

$$P_0(r) = 2P\frac{J_1(\frac{\pi r}{\lambda_{US}N})}{\frac{\pi r}{\lambda_{US}N}} \qquad (1)$$

In eq.(1) the numerical aperture $N = l_f/D$ = 3.94 and J_1 is the Bessel function of the first kind of order one.

Approximating the pressure profile with a Gaussian profile:[10]

$$P_0(r) = P\exp\left(-\frac{r^2}{w^2}\right) \quad (2)$$

one finds the characteristic width of the radial distribution $w = 0.86\,\lambda_{US}$ $N = 2.2$ mm.

As sketched in Fig.1 a glass container has been inserted into an optical goniometer of an ellipsometer (Optrel, Germany, laser wavelength $\lambda_L = 533$ nm) with the air-water or oil-water interface aligned in the center of the goniometer. US is transmitted through water. For the air-water interface we used a container open to the atmosphere; whilst for the oil-water interface we used a cylindrical cell (8 cm length and 8 cm diameter) half filled with water and half with the oil. The angle of incidence of the laser beam could be finely varied and the reflected light is detected by a four quadrant photo diode (2 × 2 cm).

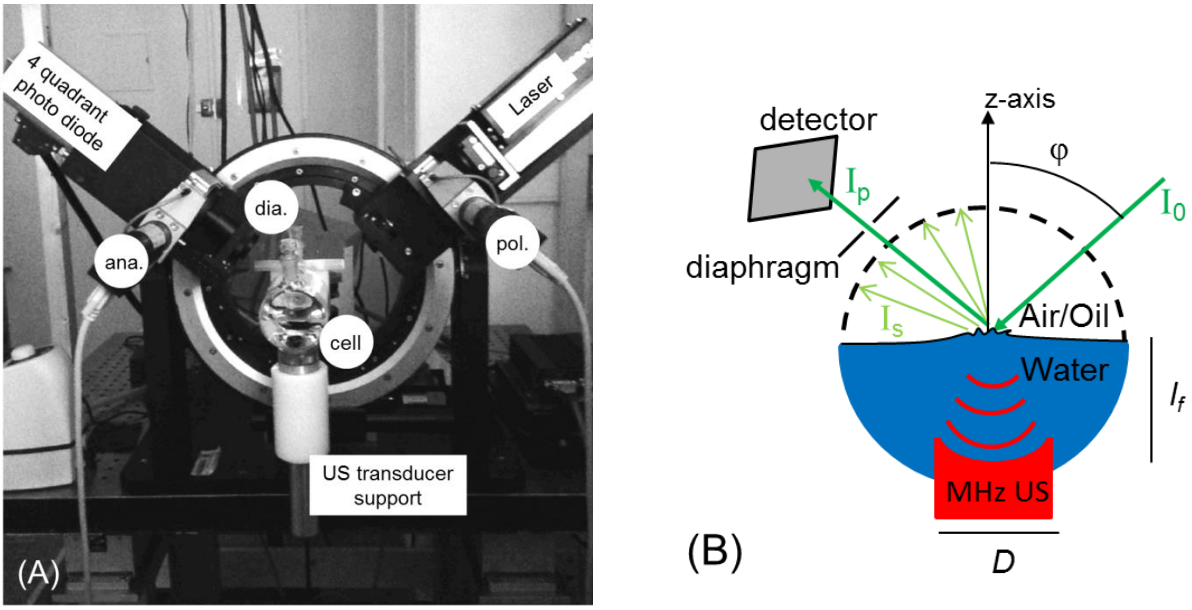

Figure 1. (A) Image of the setup composed of a four quadrant photo diode detector, laser, diaphragm (dia.), polarizer (pol.), analyzer (ana.), cylindrical cell (cell) and a US transducer mounted on a support and inserted inside the cell.

(B) Sketch of the experimental cell containing the interface. MHz ultrasound is generated inside water. A p-polarized laser beam of intensity I_0 hits the surface at an angle of incidence φ, and the reflected intensity I_p is detected. I_S is the scattered light .

2.2 ULTRASOUND AT HEPTANE-WATER AND AIR-WATER INTERFACES

MilliQ water and Heptane (Sigma Aldrich) were used as received. All experiments were carried out at room temperature ≈ 21 °C. Interfacial tension γ measurements using a pendant drop tensiometer (PAT, Sinterface) were carried out in order to check the purity of the liquids and interfaces. γ = 72.8 mN/m was measured for the air-water interface and γ = 52.6 mN/m for heptane-water in agreement with literature.

Sound speed $c = \sqrt{\frac{B}{\rho}}$, where B is bulk modulus (i.e. equal to the inverse of the adiabatic compressibility), density ρ, and the acoustic impedance $Z_0=\rho c$[11,12] in water, heptane and air are summarized in Table 1.

	ρ (Kg/m^3)	B (Pa)	c (m/s)	Z_0 (Pa s/m)	η (Pa s)
Water	997	$2.2\ 10^9$	1497	$1.49\ 10^6$	$8.9\ 10^{-4}$
Air	1.18	$1.4\ 10^5$	346	409	$18\ 10^{-6}$
Heptane	679	$8.7\ 10^8$	1130	$7.6\ 10^5$	$3.7\ 10^{-4}$

Table 1. Density ρ, bulk modulus B, sound speed c, acoustic impedance Z_0 and viscosity η in water, air and heptane.

In linear acoustics, the reflection pressure (r_{US}) and intensity (R_{US}) coefficients for normally incident ultrasound between two isotropic media are:[13]

$$r_{US} = \frac{\rho_2 c_2 - \rho_1 c_1}{\rho_2 c_2 + \rho_1 c_1}, \qquad R_{US} = \left(\frac{\rho_2 c_2 - \rho_1 c_1}{\rho_2 c_2 + \rho_1 c_1}\right)^2 \quad , \tag{3}$$

indexes 1 and 2 being for the water and air or oil, respectively.

For the water-air interface, r_{US}=–0.9997, which corresponds to total reflection condition. For water-heptane, instead, ultrasound is partially reflected and partially transmitted being r_{US}=–0.66 and R_{US}= 44 %.

In reflection, the interference of the pressure can be described as $P = P_I + P_R = \exp[i(\omega t - kz)] + r_{US}\exp[i(\omega t + kz)]$, where ω = 2π$f$ and k=2π/λ_{US}; P_I and P_R are the incident and reflected pressure, respectively. If $|r_{US}|$=1, the reflected wave has the same amplitude as the incident wave and a standing wave system is produced.[13] For a water-air interface $r_{US} \approx -1$, $P = 2\exp[i(\omega t - \pi/2)]\sin(kz)$, and the particle fluid displacement is maximum at the surface, where the pressure shows a node. The experimental case, where the pressure waves are reflected at the water-air (W-A) interface and then reflected back by the water-transducer (W-T) was studied by Issenmann.[10] Considering the effect of multiple reflections, the pressure at the interface will be given by:

$$P_i = \left[1 - r_{US,W-A} r_{US,W-T} \exp\left(i\frac{4\pi(l+h)}{\lambda_{US}}\right)\right]^{-1} P \tag{4}$$

Where l is the distance between the flat interface and the transducer and h is the height of the surface deformation. At relatively high pressures the fluid interface may also deform permanently due to the acoustic radiation pressure, and a single hump deformation could be detected as discussed in section 3.3. The single hump deformation of the fluid interface follows a profile similar to the pressure profile $P_0(r)$ generated by the transducer, see equations 1 and 2.

In our experiments, multiple reflections occur at the water-fluid and water-transducer interfaces, where equation 4 applies. The incoherent sum of multiple reflections occurring at the interface leads to a temporal and spatial deformation of the liquid surface. The temporal variation is dictated by the ultrasound frequency, whereas the characteristic spatial wavelength of these deformations respects the dispersion

relation for capillary waves accounting for gravity, viscosity and interfacial tension. Note that the effect of US attenuation is very small in our experimental systems.

Typical US power and fluid displacements investigated in this work are calculated in the following. The ultrasound intensity corresponding to the pressure maximum is $I_{US} = P^2/(2Z_0)$.[13] In water if P = 0.5 MPa, I_{US} = 83893 Pa m/s or Watt/m^2. Considering a characteristic area of $\pi w^2/2$, $I_{US} \times w^2/2$= 0.64 Watt, and the energy per unit volume is I_{US} /c = 56 Pa (if P = 0.5 MPa in water). Under the effect of US, the fluid velocity is $d\xi/dt$ = P/Z_0. In water if P = 0.5 MPa, $d\xi/dt$ = 0.3 m/s and the fluid displacement ξ = P/($2\pi f Z_0$) = 24 nm.[13]

3. RESULTS AND DISCUSSION

The profile of fluid interfaces under ultrasound has been investigated by light reflectivity and ellipsometry. Reflectivity measurements provide information on the interface profile and fluctuations at small surface wave vectors q (or large scale, $q\lambda_L \lesssim 1$, where λ_L is the laser wavelength). Fluctuations at those q scatter significantly light reducing the reflected intensity. Information on the interface profile of fluid interfaces at large wave vectors q (or short scale, $q\lambda_L \gtrsim 1$), which do not scatter significantly the light, can be revealed by ellipsometry.[14]

3.1 LIGHT REFLECTIVITY AND SURFACE ROUGHNESS

We measured the p-polarized light reflected by the air-water and heptane-water interfaces as a function of the incidence angle φ varied around the Brewster angle φ_B, at which the reflected p-polarized light is null. Upon increasing the US pressure, we observed, that the spot of the reflected light changes slightly its position but most importantly becomes more diffuse increasing about twice its size already at low pressures. These observations were made by closing completely the diaphragm in the detector arm. The presence of a diffuse spot indicates the scattering of light by the interface fluctuations due to US, whereas the reflected light deviation points to a single hump surface deformation. During the measurement, the diaphragm in the detector arm was opened enough to collect the whole reflected light spot, see Fig. 1 (and section 3.3 later).

The intensities of the reflected p-polarized light I_p for heptane-water and air-water interfaces are shown in Fig. 2 as a function of the ultrasound pressure P. In absence of US, I_p agrees with the Fresnel equation of reflection, $I_p = R_{F,p} I_0$:[14]

$$R_{F,p} = \left[\frac{\tan(\varphi_2 - \varphi_1)}{\tan(\varphi_2 + \varphi_1)}\right]^2 \qquad (5)$$

Where φ_1 is the incidence angle and φ_2 is the transmission angle, which follows Snell's law $n_1 \sin\varphi_1 = n_2 \sin\varphi_2$, where n_1 and n_2 are the refractive indexes in medium 1 and 2, respectively. n_2 = 1.33 for water, n_1= 1 for air and n_1= 1.385 for heptane.

In the fit of our data shown in Fig. 2, we introduced an angle φ_H (see Fig. 5A), which represents the deviation of the angle of incidence due to a hump deformation of the interface as explained in section 3.3. Hence the actual angle of incidence is $\varphi_1 = \varphi + \varphi_H$, where φ is the angle of incidence for a perfectly planar

interface, see Fig. 5A. When increasing the pressure of US, I_p in general (but not always) decreases as shown in Fig 2 (note that the reflectivity at P = 0.33 MPa is the lowest for the heptane-water interface). As shown in the insets of Fig. 2, for P > 0.17 MPa reflectivity curves appear flatter than the reflectivity at P = 0, which is attributed to the loss of reflected light due to scattering.

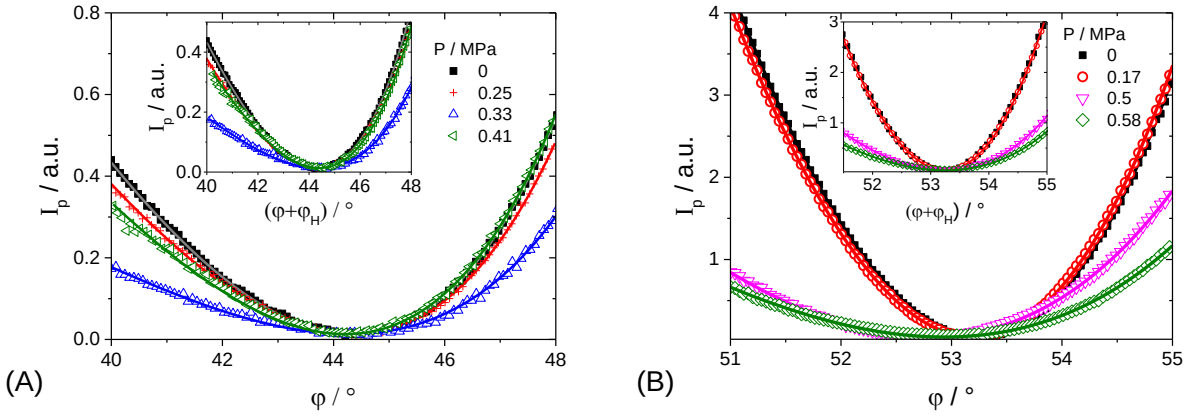

Figure 2. Reflected p-polarized intensity as a function of the angle of incidence φ, around the Brewster angle and for different pressure *P* for heptane-water (left) and air-water (right) interfaces. Insets show the reflectivity as a function of the angle $\varphi+\varphi_H$, see Fig. 5A. Lines represent the fits to the data.

For the heptane-water interface as well as for the air/water interface surface fluctuations are generated by ultrasound due to the incoherent sum of multiple reflections (see section 2.2). These fluctuations are the source of light scattering events at the interface. In order to quantify the amplitude of the surface fluctuations, we fitted the data shown in Fig. 2 following the approach of Meunier and Langevin for capillary waves.[15] Reflectivity calculation accounting for surface fluctuations at large scale with a small slope leads to:

$$\frac{I_p}{I_0} = R_p = R_{F,p}\exp(-4(k_L L)^2) \ , \qquad (6)$$

where $R_{F,p}$ is the Fresnel intensity reflection for an ideal sharp interface (equation 5), L is the root mean square amplitude of the surface roughness, and k_L is the surface light wave vector $k_L = \frac{\pi(n_1+n_2)}{\lambda}\cos(\varphi)$. The two fitting parameters in our analysis are L and the hump angle φ_H, which will be discussed in section 3.3.

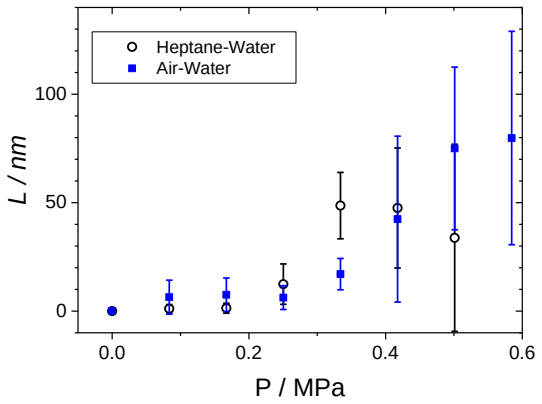

Figure 3. Surface roughness *L* as a function of the ultrasound pressure *P* for heptane-water and air-water interfaces.

Fig. 3 shows, that the amplitude of the surface roughness can reach values of about 50-100 nm at relatively low pressures, for which the permanent single hump deformation of the interface would remain small $h < 200$ µm.[10,11] It is worth noting that for thermally excited capillary waves $L \approx 0.3$ nm,[16] which is two orders of magnitude lower than the roughness for $P > 0.3$ MPa . Moreover, the oscillation of the fluid displacement induced by US, $\xi = P/(2\pi f Z_0) = 24$ nm (if P=0.5 MPa) and L shown in Figure 3 are comparable.

Now we attempt to estimate the characteristic wavelength λ_s of the surface mode $q_s = 2\pi/\lambda_s$ produced under the effect of US radiation. Following the approach of Fogler,[2] which described the behavior of fluid interfaces in the different steps of acoustic emulsification, the dispersion relation of the surface waves accounting for the capillary, inertial and viscous contributions for low viscosity liquids follows :

$$\frac{4q_s^3}{\omega^2(\rho_1+\rho_2)^2}[\gamma(\rho_1+\rho_2) - 4q_s(\eta_1+\eta_2)^2] = 1 \quad . \qquad (7)$$

Here $\omega = 2\pi f = 14.1$ MHz, and $q_s = 0.88$ µm^{-1} ($\lambda_s = 7.1$ µm) for water-air and $q_s = 1.2$ µm^{-1} ($\lambda_s = 5.2$ µm) for water-heptane. The latter $q_s$values correspond to $q_s \lambda_L \lesssim 1$, and confirm that surface fluctuations at low wave vectors are the source of the reflectivity loss due to light scattering by surface fluctuations.

Accounting for inertial and viscous forces generated by ultrasound at the interface, a critical amplitude α_c of the vibration of the acoustic field, above which the surface modes generated by US become unstable, can be also calculated:[2]

$$\alpha = \frac{g_0}{\omega^2} > \alpha_c = \frac{4q_s(\eta_1+\eta_2)}{\omega(\rho_2-\rho_1)}, \qquad (8)$$

where g_0 is the amplitude of the inertial force function $g_0\cos(\omega t)$. Here, $\alpha_c = 229$ nm for water-air and $\alpha_c = 1.36$ µm for water-heptane. Above this instability threshold, the acoustic fountain phenomenon would be expected, leading to the generation of droplets. Note that the surface roughness L shown in Fig. 3 is always lower than the critical value, for which the interface becomes unstable. Hence in our experiments,

ultrasound generates surface modes (surface roughness) with characteristic wavelengths λ_s of the order of few microns and amplitude as high as 100 nm (see Fig 3).

3.2 ELLIPSOMETRY

Information on the interface at short scale, which does not scatter light, can be revealed by ellipsometry. We measured the ellipsometric amplitude Ψ and phase shift Δ close to the Brewster angle (40° < φ < 48° for heptane-water and 50° < φ <56° for air-water) and obtained the real and imaginary parts of the ratio of the field reflection coefficient of the p- and s- polarized light:

$$\frac{r_p}{r_s} = \tan\Psi\cos\Delta + i \cdot \tan\Psi\sin\Delta = \mathrm{Re}\left(\frac{r_p}{r_s}\right) + i \cdot \mathrm{Im}\left(\frac{r_p}{r_s}\right) \quad . \tag{9}$$

From the imaginary part, $\mathrm{Im}(\frac{r_p}{r_s}) = \tan\Psi\sin\Delta$, we calculate the perturbation parameter O_1, which describes the deviation of the interfacial profile from a perfectly sharp optical profile:

$$\mathrm{Im}\left(\frac{r_p}{r_s}\right) = \frac{\pi\sqrt{n_1^2+n_2^2}}{\lambda_L(n_1^2-n_2^2)} O_1 \tag{10}$$

$$O_1 = \int_{-\infty}^{\infty} \frac{(n_\perp^2(z)-n_1^2)(n_\perp^2(z)-n_2^2)}{n_\perp^2(z)} + (n_\parallel^2(z)-n_\perp^2(z))\ dz \approx \int_{-\infty}^{\infty} \frac{(n^2(z)-n_1^2)(n^2(z)-n_2^2)}{n^2(z)}\ dz, \tag{10}$$

where for an isotropic interfacial profile $n(z)$, the refractive indices parallel $n_{||}$ and perpendicular $n_\perp$ to the interface are equal. Note that for a refractive index profile $n(z)$ changing sharply from n_1 to n_2, $O_1 = 0$. For simple liquids, the interfacial profile can be described by an isotropic refractive index varying from n_1 to n_2. In this case the perturbation parameter is negative, $O_1 < 0$, see equation 10. For aqueous interfaces, however, some experimental investigations reported $O_1 > 0$.[17–19,20] These results may be attributed to the complex interactions and structure of interfacial water. For instance, it is well known from spectroscopic investigations, that the water structure becomes ordered at the interface with some OH groups pointing towards the fluid interface as in ice-water.[21,22] In absence of US, O_1 is called O_0 ($P = 0$). Here we also measured a positive perturbation parameter $O_0 = 0.1\pm0.1$ nm[17] for the air-water interface ($O_0 \approx 0\pm0.1$ nm for the heptane-water interface), that cannot be described by models accounting only for surface roughness.[23]

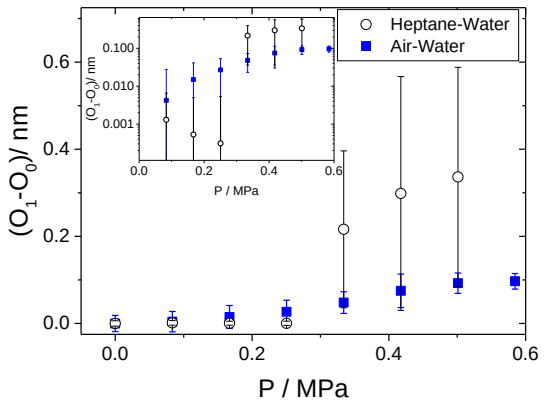

Figure 4. Ellipsometric perturbation parameter $O_1 - O_0$ as a function of the US pressure for heptane-water and air-water interfaces.

In fig. 4, we plot the difference between the perturbation parameter measured in presence (O_1) and in absence of US (O_0). The perturbation parameter O_1 increases when the ultrasound pressure P is increased for air-water interfaces; whereas, it is approximately null for $P < 0.3$ MPa and it increases for $P > 0.3$ MPa at the heptane-water interface. Note that the error bars for heptane-water interfaces are quite large given that the refractive indices of heptane and water are close (see section 3.1). According to eq. 10, an increase of O_1 would correspond to an interfacial structure optically denser than both fluids, $n(z) > n_1$ and $n(z) > n_2$;[20] or for oil-water interfaces, an increase of a depletion layer due to repulsion between water and hydrophobic molecules, $n(z) < n_1$ and $n(z) < n_2$.[18] Assuming a degree of anisotropy, our observation in absence of US, $O_0 = 0.1 \pm 0.1$ nm, can be explained by $n_{||} = 1.309$ and $n_{\perp} = 1.154$ and a thickness of 0.4 nm for the air-water interface.[17] Hence, assuming that the refractive index remains the same under US, our results $O_1 = 0.1$-0.3 nm points to an increase of two or three fold of the interfacial width of bare interfaces, up to 0.8-1.2 nm.

3.3. PERMANENT SINGLE HUMP DEFORMATION ANALYSIS

In Fig. 2, we also observed a small but significant shift of the angle at which the minimum of the intensity is measured and we introduced a fitting parameter φ_H, which accounts for this shift, see Fig. 5A. In Fig. 5B we plotted the absolute value of the fitting parameter φ_H as a function of the ultrasound pressure P. Note that we found positive and negative value of φ_H, which implies that the changes observed cannot be attributed to a decrease of the bulk refractive index of water due to cavitation. For $P < 0.2$ MPa the shift remains small, $\varphi_H < 0.1°$; but it becomes significant $\approx 0.4°$ at the highest pressures investigated.

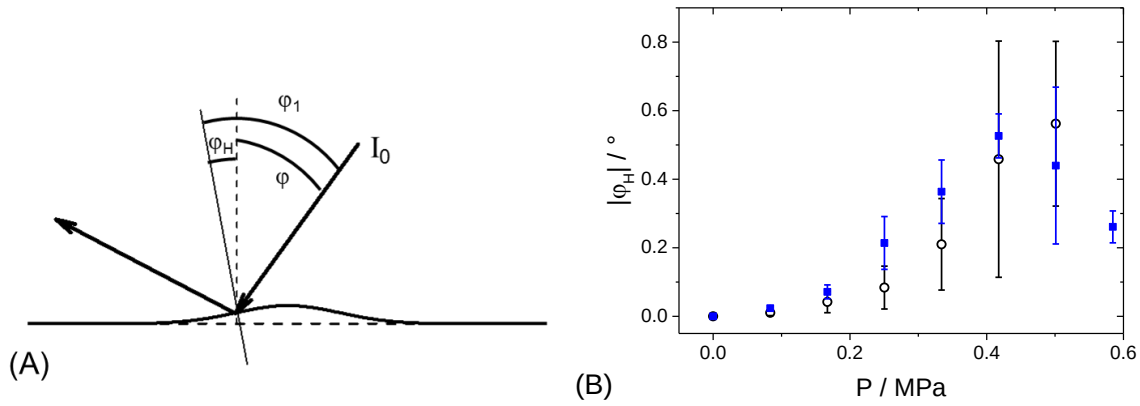

Figure 5. (A) Sketch of the angle of incidence in the presence of a hump deformation of the fluid interface (B) Absolute value of the hump angle φ_H as a function of pressure *P*.

This shift can be related to a shift of the angle of incidence related to a single hump deformation of the interface due to the radiation pressure, which modifies the angle of incidence of the interface as sketched in Fig. 5A. At the air-water interface, the radiation pressure $\Pi=P_i^2/(\rho c^2)$ is the driving pressure for the surface deformation, which is counterbalanced by gravity and capillarity:[10]

$$\rho g h(x,y) - \gamma\kappa(x,y) = \Pi(x,y) \qquad (11)$$

In eq. (11) γ is the interfacial tension, κ is the curvature of the deformation. For typical values of h and curvature, the capillary term is always the leading term. The hump has a characteristic size of about w_H = 2.2 mm (see section 2.1). A characteristic height h_H of the hump can be estimated assuming a triangular shape: $h_H = w_H \tan(\varphi_H)$= 15 µm if φ_H = 0.4°, which is relatively small comparing to other reported values at higher pressure.[10] Since the typical lateral size of the hump is 2.2 mm, whereas the laser spot is about 0.5 mm size, we can consider that the laser spot is small enough to see the hump as locally planar.

We now check, if an interpretation alternative to the surface roughness analysis (section 3.1) can be proposed to describe our data (Figs 2-5). In the following we suppose, that no capillary waves or other surface waves are generated under US, but the surface is deformed only with a single hump.[10] First, we consider that the hump could also enlarge the reflected laser spot. Note that in this case the reflected intensity collects a range of angles of incidence; and one would expect that at the Brewster angle, the reflected intensity is significantly larger than zero, since for angles lower and higher than the Brewster angle the intensity is non null. However, we did not observe a change of the intensity minimum values, and we can safely discard an interpretation of our results in terms of spreading of the angle of incidence. One could also imagine that some light is simply lost, because the reflected beam is significantly deviated by the hump and not collected by the detector. Actually from φ_H shown in Fig. 5B, the angle of incidence may deviate by 0.1-0.5°. In a limiting case, the spot of the reflected light on the detector will be shifted by $l_p\, 2\varphi_H$, where l_p is the distance between the interface and the detector. Here l_p =30 cm and $l_p\, 2\varphi_H$ = 5 mm, which is smaller than the size of 2 cm of the photodiode detector. Hence even for the maximum possible

surface deformation the detector collects the whole reflected beam and a single hump deformation cannot explain our results. The effect of acoustic cavitation is also discussed in the Appendix and shown to be rather improbable in view of the too high energies needed at these relatively low acoustic pressures.

4. CONCLUSIONS AND OUTLOOK

In this work, we have investigated the surface roughness of water-oil and water-air interfaces induced by MHz ultrasound in a range of relatively low ultrasound intensities. Surface fluctuations at large scales scatter significantly the light incident to the surface. By light reflectivity we measured a surface roughness as high as 50-100 nm, if the US pressure is increased up to $P = 0.5$ MPa. Hence, the effective contact area between two fluids can be increased dramatically by US, which is expected to have a pronounced impact on interface based separation processes like liquid-liquid extractions. At small scale we measured by ellipsometry modest increments of the interfacial width. In the future, we plan surface light scattering experiments resolved in time and space in order to get information on the spectrum of surface waves induced by ultrasound and to measure directly the frequency and the damping of those waves by varying the scattering vector in the interfacial plane. Another future prospect will be to study, how much the increase of interface roughness can accelerate the rate interfacial reactions like phase transfer.

ACKNOWLEDGEMENTS

We thank Thomas Zemb for discussions and encouraging developing this work. We thank also Rachel Pflieger for some advices on US calibration. Labex CheMISyst is acknowledged for the financial support as well as the ERC Grant Agreement Nr. 320915 "REE-CYCLE": Rare Earth Element reCYCling with Low harmful Emissions. A.S. thanks Benjamin Dollet, Bruno Issenmann and Angelo Pommella for discussions.

REFERENCES

(1) Friend, J.; Yeo, L. Y. Microscale Acoustofluidics: Microfluidics Driven via Acoustics and Ultrasonics. *Rev. Mod. Phys.* **2011**, *83* (2), 647–704.

(2) Li, M. K.; Fogler, H. S. Acoustic Emulsification. Part 1. The Instability of the Oil-Water Interface to Form the Initial Droplets. *J. Fluid Mech.* **1978**, *88*, 499.

(3) Peskin, R.; Raco, R. Ultrasonic Atomization of Liquids. *J. Acoust. Soc. Am.* **1963**, *35*, 1378.

(4) Li, M. K.; Fogler, H. S. Acoustic Emulsification. Part 2. Breakup of the Large Primary Oil Droplets in a Water Medium. *J. Fluid Mech.* **1978**, *88*, 513.

(5) Lang, R. Ultrasonic Atomization of Liquids. *J. Acoust. Soc. Am.* **1962**, *34*, 6.

(6) Suslick, K. S. Ultrasound: Its Chemical, Physical, and Biological Effects. *VCH Publ. New York.* **1988**.

(7) Kaci, M.; Meziani, S.; Arab-Tehrany, E.; Gillet, G.; Desjardins-Lavisse, I.; Desobry, S. Emulsification by High Frequency Ultrasound Using Piezoelectric Transducer: Formation and Stability of Emulsifier Free Emulsion. *Ultrason. Sonochem.* **2014**, *21*, 1010–1017.

(8) Reddy, S. R.; Fogler, H. S. Emulsion Stability of Acoustically Formed Emulsions. *J. Phys. Chem.* **1980**, *84* (12), 1570–1575.

(9) Radziuk, D.; Möhwald, H. Ultrasonically Treated Liquid Interfaces for Progress in Cleaning and Separation Processes. *Phys. Chem. Chem. Phys.* **2015**, *18* (1), 21–46.

(10) Issenmann, B.; Wunenburger, R.; Manneville, S.; Delville, J.-P. Bistability of a Compliant Cavity Induced by Acoustic Radiation Pressure. *Phys. Rev. Lett.* **2006**, *97* (7), 074502.

(11) Issenmann, B.; Wunenburger, R.; Chraibi, H.; Gandil, M.; Delville, J.-P. Unsteady Deformations of a Free Liquid Surface Caused by Radiation Pressure. *J. Fluid Mech.* **2011**, *682*, 460–490.

(12) Luning Prak, D. J.; Alexandre, S. M.; Cowart, J. S.; Trulove, P. C. Density, Viscosity, Speed of Sound, Bulk Modulus, Surface Tension, and Flash Point of Binary Mixtures of N -Dodecane with 2,2,4,6,6-Pentamethylheptane or 2,2,4,4,6,8,8-Heptamethylnonane. *J. Chem. Eng. Data* **2014**, *59* (4), 1334–1346.

(13) Leighton, T. G. *The Acoustic Bubble*; 1994; Vol. 96.

(14) Langevin, D. Light Scattering by Liquid Surfaces and Complementary Techniques. *Surfactant science series*. 1992, p 451.

(15) Meunier, J.; Langevin, D. Optical Reflectivity of a Diffuse Interface. *J. Phys.* **1982**, *43*, 185.

(16) Bonn, D.; Wegdam, G. Capillary Waves and Ellipsometry Experiments. *J. Phys.* **1992**, *2*, 1755.

(17) Stocco, A.; Tauer, K. High-Resolution Ellipsometric Studies on Fluid Interfaces. *Eur. Phys. J. E. Soft Matter* **2009**, *30* (4), 431–438.

(18) Day, J.; Bain, C. Ellipsometric Study of Depletion at Oil-Water Interfaces. *Phys. Rev. E* **2007**, *76* (4), 041601.

(19) Beaglehole, D. Structural Changes in the Surface of Water. *J. Phys. Chem.* **1987**, *91* (19), 5091–5092.

(20) Greef, R.; Frey, J. G. The Water-like Film on Water. In *Physica Status Solidi (C) Current Topics in Solid State Physics*; 2008; Vol. 5, pp 1184–1186.

(21) Moore, F. G.; Richmond, G. L. Integration or Segregation: How Do Molecules Behave at Oil/water Interfaces? *Acc. Chem. Res.* **2008**, *41* (6), 739–748.

(22) Shen, Y. R.; Ostroverkhov, V. Sum-Frequency Vibrational Spectroscopy on Water Interfaces: Polar Orientation of Water Molecules at Interfaces. *Chem. Rev.* **2006**, *106* (4), 1140–1154.

(23) Meunier, J. Optical Reflectivity of Thin Rough Films: Application to Ellipsometric Measurements on Liquid Films. *Phys. Rev. E - Stat. Nonlinear, Soft Matter Phys.* **2007**, *75* (6).

(24) Herbert, E.; Balibar, S.; Caupin, F. Cavitation Pressure in Water. *Phys. Rev. E - Stat. Nonlinear, Soft Matter Phys.* **2006**, *74* (4), 1–22.

APPENDIX

CAVITATION

In our experiments milliQ water was used without degassing. Hence, one may wonder if acoustic cavitation occurs in the range of pressures investigated here. Cavitation in distilled water depends on many parameters as the dispersed gas concentration, impurities and wall effects. Reported cavitation pressures for distilled water range from –0.1 to –20 MPa.[24]

The energy related to homogenous cavitation in a liquid can be written:

$$E(R) = \frac{4}{3}\pi R^3 (P - P_{sat}) + 4\pi R^2 \gamma \qquad \text{(A1)}$$

In eq. A1, R is the bubble radius, P is the pressure and P_{sat} is the saturation pressure. We plot $E(R)$ for typical pressure values investigated here in Fig. A1.

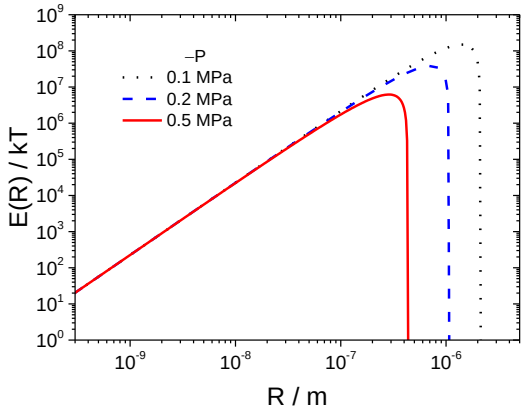

Figure A1. Free energy of a cavitation bubble as a function of the pressure P in equation A1.

A critical value of the bubble radius R_c, above which the bubble may grow corresponds to the radius for which $E(R)$ is maximum. For pressure of –0.5 MPa, critical radii $R_c \approx 300$ nm and the activation energy is about 6 10^6 kT. The sizes of these critical radii are relatively large and the cavitation probability to occur is quite low.[24] Hence we can safely conclude that cavitation is not expected to occur and affect our experiments given the relatively small pressure range investigated here, the relatively large critical radius and the purity of our liquids checked by interfacial tension experiments.

TABLE OF CONTENTS GRAPHIC